AGU PUBLICATIONS

JGR

Journal of Geophysical Research: Solid Earth

RESEARCH ARTICLE
10.1002/2016JB013001

Key Points:
- Clustered arrivals of $M_w < 2$ low-frequency earthquake signals (LFEs) can explain characteristics of very low frequency (VLF) events
- Temporally clustered LFE sources may be triggered by a single larger or many smaller distinct aseismic slip events, or occur by chance
- VLF events may not bridge the gap between $M_w > \sim 5$ slow slip transients and LFEs

Correspondence to:
J. Gomberg,
gomberg@usgs.gov

Citation:
Gomberg, J., D. C. Agnew, and S. Y. Schwartz (2016), Alternative source models of very low frequency events, *J. Geophys. Res. Solid Earth*, *121*, 6722–6740, doi:10.1002/2016JB013001.

Received 16 MAR 2016
Accepted 1 SEP 2016
Accepted article online 4 SEP 2016
Published online 24 SEP 2016

Alternative source models of very low frequency events

J. Gomberg[1], D. C. Agnew[2], and S. Y. Schwartz[3]

[1]U.S. Geological Survey, University of Washington, Seattle, Washington, USA, [2]Institute of Geophysics and Planetary Physics, University of California, San Diego, La Jolla, California, USA, [3]Department of Earth and Planetary Sciences, University of California, Santa Cruz, California, USA

Abstract We present alternative source models for very low frequency (VLF) events, previously inferred to be radiation from individual slow earthquakes that partly fill the period range between slow slip events lasting thousands of seconds and low-frequency earthquakes (LFE) with durations of tenths of a second. We show that VLF events may emerge from bandpass filtering a sum of clustered, shorter duration, LFE signals, believed to be the components of tectonic tremor. Most published studies show VLF events occurring concurrently with tremor bursts and LFE signals. Our analysis of continuous data from Costa Rica detected VLF events only when tremor was also occurring, which was only 7% of the total time examined. Using analytic and synthetic models, we show that a cluster of LFE signals produces the distinguishing characteristics of VLF events, which may be determined by the cluster envelope. The envelope may be diagnostic of a single, dynamic, slowly slipping event that propagates coherently over kilometers or represents a narrowly band-passed version of nearly simultaneous arrivals of radiation from slip on multiple higher stress drop and/or faster propagating slip patches with dimensions of tens of meters (i.e., LFE sources). Temporally clustered LFE sources may be triggered by single or multiple distinct aseismic slip events or represent the nearly simultaneous chance occurrence of background LFEs. Given the nonuniqueness in possible source durations, we suggest it is premature to draw conclusions about VLF event sources or how they scale.

1. Introduction

"Very low frequency" events refer to pulses of energy observed in seismic data in the 0.02–0.05 Hz frequency band. These have been thought to represent seismic waves radiated from fault slip events with magnitude M_w2–5 with lower stress drops and slower rupture velocities than ordinary earthquakes. Hereafter, we use the common nomenclature VLF events to refer to these transient signals, while proposing alternative interpretations of what processes they may result from. Numerous authors have suggested that the sources of VLF events bridge the period gap between transient slow slip events with large moments ($M_0 > \sim 10^{17}$ N m or moment magnitude $M_w > \sim 5.5$) and durations of days to years, and low-frequency earthquakes, with very small moments ($M_0 < \sim 10^{12}$ N m or $M_w < \sim 2.0$) and durations of fractions of a second. The former radiate negligible seismic energy and typically is measured geodetically, while the latter are inferred to rupture slowly relative to ordinary earthquakes of the same moments but still fast enough to radiate measurable seismic signals [*Ide et al*., 2007a, 2007b, 2008; *Ito et al*., 2009; *Matsuzawa et al*., 2009; *Takeo et al*., 2010; *Ide and Yabe*, 2014]. These small events are called low-frequency earthquakes (LFE) because they are depleted in high-frequency energy relative to typical earthquakes with comparable low-frequency spectral amplitudes.

Here we introduce a few features of LFE signals relevant to this study, with more discussion provided in section 2. LFE occurrence and transient slow slip appear to be causally linked based on correlations between their rates and estimated source locations, and both are inferred to represent release of tectonic stresses via shear slip along plate interfaces, with the slow slip being the primary mode of release [*Ide et al*., 2007a; *Frank et al*., 2013; *Royer and Bostock*, 2014]. LFE signals also appear to cluster spatially and temporally [*Shelly et al*., 2007; *Frank et al*., 2014; *Sweet et al*., 2014; *Bostock et al*., 2015; *Savard and Bostock*, 2015; *Frank et al*., 2016] and are thought to be the building blocks of tremor, a term which describes emergent, quasi-continuous, low-amplitude, seismic signals that correlate over distances of tens of kilometers or more [*Shelly et al*., 2006].

We present an alternative model for the origin of VLF events. We suggest that, instead of representing the seismic radiation from M_w2–5 slow earthquakes, some VLF events may be simply the result of narrowband filtering of clustered arrivals of much smaller signals from $M_w < 2$ LFEs. In a single slip event, the physics of dynamic rupture governs a process of coherent slip propagation, and the temporal and spatial scales of this

process determine the characteristics of the radiated seismic energy. The complete spectrum of waves radiated from an event propagating coherently over tens of kilometers and hundreds of seconds will differ from the spectrum of a sum of smaller slip events, each propagating only tens of meters within fractions of a second. But as we show, this difference may not be distinguishable using only observations in narrow-frequency bands. To highlight the nonuniqueness in interpretation of such observations, we note here that while linking VLF events with tremor bursts is common to both the models we propose the one presented in *Ide* [2008], the models differ in fundamental ways; in particular, Ide's model [*Ide*, 2008] suggests that VLF events represent radiation directly resulting from larger slow slippage and that LFE signals may be artifacts of limited detection capabilities (see section 6 for more discussion).

We illustrate the difference between sources of a single, larger slip event and a sum of smaller ones by considering the more familiar and analogous cases of aftershocks and afterslip, and earthquake swarms and accompanying slow, aseismic slip. Repeating earthquakes also are now often used to infer characteristics of driving slow, aseismic slip [*Nadeau and McEvilly*, 1999; *Gardonio et al*., 2015; *Lengliné and Ampuero*, 2015]. In general, the moment of the aseismic slip substantially exceeds that of cumulative moment of the seismic events, and thus, the former likely drives the latter [*Peng and Gomberg*, 2010]. Often, only the seismic signals are observable, and while they provide clues that aseismic slip is underway, one would not use the envelope of the aftershocks, repeaters, or swarm earthquakes to infer details or even gross features (e.g., the total moment) of the afterslip or driving slow slip.

If LFEs are a response to transient slow slip, similar caution should be employed when using their aggregate signals to infer the characteristics of whatever drives them, particularly when only a narrow frequency band of the aggregate signal is examined. Simulation of moderate to large earthquakes also illustrates the important distinction between a single larger slip event and a cascade or sum of smaller ones. Nearly all methods to simulate earthquakes as distributed sources invoke a discretized form of the representation theorem, which describes the displacement field at some distance from the fault as an integral over the fault plane of the product of the slip history and a Green's function describing the medium response [*Aki and Richards*, 1980]. Small earthquake seismograms may be used as Green's functions distributed over points on the rupture plane, weighted and filtered by a model of the slip history (source model) at each corresponding point (see *Hartzell et al*. [1999] for a summary). A source model representing the coherent propagation of slip determines the weightings and phase shifts used to sum the Green's functions and is required to reproduce the complete spectrum correctly [*Frankel*, 1995; *Hartzell et al*., 1999]. Summing independent, randomly distributed LFE signals is equivalent to using random weightings and phase shifts, effectively using no source model. It would then make no sense to measure the summed signals and infer a source model, as one does not exist.

In section 2 we describe the characteristics of VLF and LFE observations and of tremor that any interpretations should explain or be consistent with. We then present an analytic model of a clustered series of LFE signals (section 3), simulations using synthetic signals (section 4), and a test using observations of tremor and VLF events from Costa Rica (section 5).

2. VLF, LFE, and Tremor Characteristics

VLF events refer to pulses of seismic energy with durations of tens to several hundred seconds, inferred to represent waves radiated from fault slip events with $M_w \sim 2$–5 (Figure 1, modified from *Ito et al*. [2007]), which contrast with LFE signals that originate from smaller slow earthquakes ($M_w \sim -1$ to 1.5), which last less than a few seconds, and radiate most often in the 2–8 Hz passband (see the Introduction in *Sweet et al*. [2014] for more background). Characteristics attributed to the inferred source of VLF events include significantly lower stress drops and/or slower rupture velocities than ordinary earthquakes. Tremor also belongs to the class of slow earthquakes, and a number of studies have suggested that tremor may be composed of a superposition of LFE signals [*Shelly et al*., 2006, 2007; *Ide et al*., 2008; *Chamberlain et al*., 2014; *Frank et al*., 2014]. In some studies the spectra of these slow seismic signals appear to decay as $\sim f^{-1}$ rather than $\sim f^{-2}$ measured for many fast earthquakes [*Ide et al*., 2007b; *Rubinstein et al*., 2010], and in others both tremor and fast earthquakes decay as $\sim f^{-2}$ [*Fletcher and McGarr*, 2011; *Zhang et al*., 2011]. In various ways these studies attempted to account for the spectral decay due to attenuation. [*Gomberg et al*., 2012] showed that in some instances spectral decay rate differences between earthquakes and LFEs may be attributed to near-source attenuation rather than source differences.

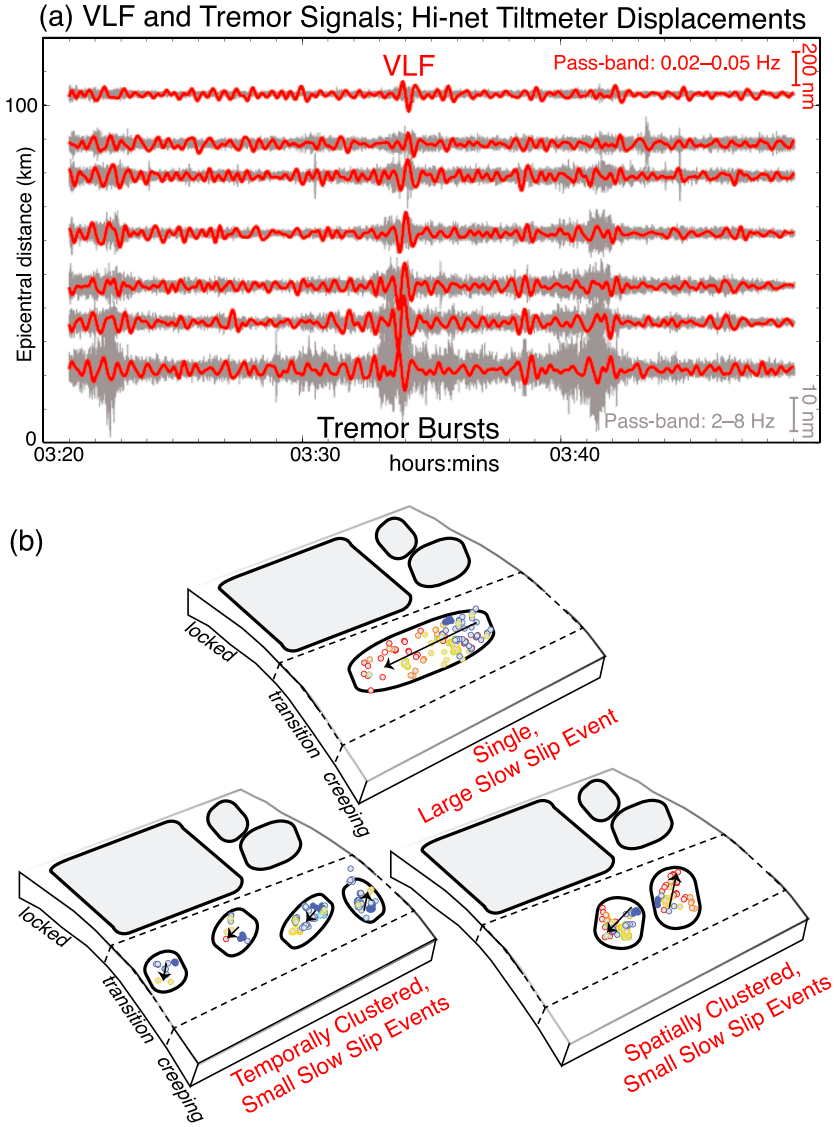

Figure 1. Examples of VLF waveforms and inferred source models. (a) Displacement waveforms derived from radial-component tiltmeter signals recorded by the Japanese Hi-net network at a range of source-receiver distances, after band-pass filtering in the 0.02–0.05 Hz (red) and 2–8 Hz (gray) passbands to illuminate VLF events and tremor, respectively. Modified from *Ito et al.*'s [2007] Figure 1. (b) Cartoons of fault surfaces, with features of *Ito et al.*'s [2007] Figure 4, with three different LFE source models that might give rise to indistinguishable clustered LFE arrivals, tremor bursts, and VLF events. A velocity-strengthening background contains velocity-weakening patches. In the shallower "locked" zone, large patches (gray polygons) slip in earthquakes. In the transition zone slip occurs in transient, mostly aseismic slow slip episodes within outlined polygons that contain tiny patches (circles with colors and arrows indicating relative failure times). See text.

Another noteworthy characteristic of VLF events is that in almost all cases they are observed with concurrent tremor, particularly during bursts of tremor activity [*Ito and Obara*, 2006a; *Ito et al.*, 2007; *Ide et al.*, 2007a, 2007b, 2008; *Ito et al.*, 2009; *Matsuzawa et al.*, 2009; *Takeo et al.*, 2010; *Walter et al.*, 2013; *Frank et al.*, 2014; *Ide and Yabe*, 2014; *Ghosh et al.*, 2015; *Savard and Bostock*, 2015; *Yamashita et al.*, 2015; *Ide*, 2016]. *Ide et al.* [2008] identified and measured VLF events by fitting theoretical moment-rate functions to seismic displacement data band-pass filtered between 0.005 and 0.05 Hz during time intervals with clear tremor and noted that the moment-rate functions estimated have nearly identical shapes to the envelopes of the squared seismic velocities in the tremor bandpass of 2–8 Hz. Notably, they inferred that VLF event sources and LFEs most likely are each triggered by concurrent surrounding, slower, and larger slip, but they also noted that the VLF events could be a superposition of those from LFEs. *Ide and Yabe* [2014] used the timing

of tremor bursts to stack broadband seismograms in order to detect VLF events in western Japan. Their stacking procedure revealed that high-frequency tremors are accompanied by VLF events in all regions with tremor in western Japan and that the seismic energy of the tremor and the seismic moment in the VLF band are proportional. They argued that the ubiquity of VLF events provides support for the idea of a continuum of slow slip phenomena from the tremor band through the geodetic observations of slow slip. Finally, *Ide* [2008] proposed a model linking VLF events to LFEs and tremor, which we discuss more thoroughly in section 5.

The studies of *Ito et al*. [2007, 2009], *Matsuzawa et al*. [2009], and *Takeo et al*. [2010] also suggest that LFEs and sources of VLF events are members of a continuum of slow slip events. The two studies of *Ando et al*. [2012], *Asano et al*. [2008], and *Hutchison and Ghosh* [2016] identified VLF events but not tremor. However, in the Asano and Ando studies the occurrence of tremor accompanying their VLF observations from Japan cannot be ruled out, at least based on information provided, because neither publication mentions a search for tremor [*Asano et al*., 2008; *Ando et al*., 2012]; their analyses focused on data filtered in the VLF passband of 0.02–0.05 Hz and only examined data at frequencies in the tremor passband ($>$1 Hz) to search for potentially contaminating earthquakes, without specifying how the search was conducted [*Ando et al*., 2012] or searching only in time windows when earthquakes were cataloged [*Asano et al*., 2008]. Moreover, the results reported in *Ando et al*. [2012] may indicate that the VLF events were sums of LFEs that originated from multiple locations and arrived in clusters, as they noted "complicated waveforms" for over 50% of the 1314 VLF events identified and of the 120 with locations and focal mechanisms estimated, only 18% was considered robust and 27% had complex waveforms and scattered locations. *Hutchison and Ghosh* [2016] found eight VLF events during an ~90 day interval during the 2014 Cascadia "episodic tremor and slip" event, which located in a region lacking "strong" tremor activity. The low signal to noise and monochromatic nature of the data, coupled with poor fits between data and synthetic waveforms (variance reduction of 47%) for the single example of a centroid moment tensor inversion of a VLF event shown, casts some doubt on these findings. Notably, perhaps, *Hutchison and Ghosh* [2016] conclude that "while we cannot entirely rule out that some of the initial detections are, in fact, real, we only include events with robust moment tensor solutions."

If tremor is composed of LFE signals (see next paragraph and *Shelly et al*. [2006]), then arrivals of spatially and/or temporally clustered LFE signals would manifest as tremor bursts and possibly VLF events. Indeed, while detection methods that rely on correlation and waveform similarity will pick out LFEs with spatially clustered sources [*Bostock et al*., 2012; *Frank et al*., 2014; *Royer and Bostock*, 2014; *Bostock et al*., 2015; *Frank et al*., 2016], they also commonly cluster temporally as well [*Shelly et al*., 2007; *Frank et al*., 2014; *Sweet et al*., 2014; *Bostock et al*., 2015; *Savard and Bostock*, 2015; *Frank et al*., 2016]. *Sweet et al*. [2014] studied recurring clusters, or "families," in Cascadia and found a single family would be active for 10 min to 12 h. In their analysis of LFE families in Mexico, *Frank et al*. [2014] found LFE families activated in bursts, with interevent recurrence intervals of $<$10 s.

We propose that in some cases, VLF events result from temporally clustered arrivals of LFE signals, suggested by the fact that VLF events almost always are simultaneous with tremor bursts. This proposition thus relies on the assumption that tremor is a superposition of LFE signals, as first proposed in *Shelly et al*. [2006]. We justify this assumption with a brief review of the evidence for it. To our knowledge, in most studies LFEs detected within tremor comprise only a fraction of the tremor, but we suggest that it is impossible to know whether this reflects physical processes or detection biases. For example, in their study of LFEs in Guerrero, Mexico, *Frank et al*. [2014] found only 35% of the tremor contained LFEs. LFEs appear to be more abundant in the northern portions of Cascadia, but nowhere account for all the tremor [*Bostock et al*., 2015; *Savard and Bostock*, 2015]. Nearly all LFE detection methods impose restrictive detection criteria, thus implicitly selecting only a subset of LFEs and resulting in an incomplete LFE catalog. These methods rely on waveform similarity, either at multiple recording stations in a network (e.g., beam-forming methods) and/or between LFEs at multiple times (e.g., match-filtering and stacking methods). The requirement for cross-station similarity means detections is possible only when propagation and site effects are similar at network stations, proposed as an explanation for the geographic variation in LFE rates in Cascadia [*Rubin and Armbruster*, 2013; *Armbruster et al*., 2014; *Savard and Bostock*, 2015]. Methods reliant on waveform similarity between multiple LFEs will detect only sources that recur with nearly the same location and mechanism. The results of *Frank et al*. [2014] suggest that this may eliminate many LFEs that do not repeat, noting that their application of a beam-forming method yielded many thousands of LFE detections but an "enormous amount of events" did not meet the coherence requirements of their second-step stacking procedure. In addition to detection

biases, real physical processes may hamper the ability to unravel individual LFEs from tremor and lead to real variations in how LFEs cluster temporally and spatially. The source dimensions of LFEs, and how they scale and recur, likely depend on differential stresses and frictional properties, properties that surely vary temporally and spatially [*Wech and Creager*, 2011; *Bostock et al*., 2015]. Additionally, the amplitudes radiated by LFEs may reflect variations in the slow slip inferred to drive them, which surely also varies temporally and spatially [*Bostock et al*., 2015].

Finally, we consider how clustering may arise, noting that many ways appear plausible, making it difficult to infer uniquely what slow slip may drive it [*Sweet et al*., 2014; *Bostock et al*., 2015; *Frank et al*., 2016]. Figure 1b illustrates just a few of the models of LFE sources and driving slow slip that might radiate signals that arrive in similarly clustered bursts. These models are based on ideas of *Ide* [2014] and other studies referenced therein, in which the properties of the fault surface may be described by elastic, velocity-weakening patches (gray areas within polygons or gray and blue shaded tiny circles) within a viscous, velocity-strengthening background, and in which fracture energy increases with patch size [*Ide*, 2014]. In the shallower "locked" zone, large patches cover most of the surface so tectonic stress relaxation occurs primarily through fast, dynamic slip with relatively large stress drops (i.e., earthquakes). In the "transition" zone, the properties of the background dominate and transient, slow, essentially aseismic slip with low stress drops relax tectonic stressing. Low-amplitude LFE signals radiate from the tiny patches whose failure is triggered by the passing slow slip front, either immediately or with some delay. LFEs may radiate waves that arrive in clustered bursts, but originating from a variety of different temporal and spatial source distributions (illustrated schematically in Figure 1b). The driving process underlying each of these distributions may differ quite significantly.

The study of *Frank et al*. [2016] suggests an important, but indirect role of slow slip in the evolution of LFE activity. They study LFE activity in Mexico and conclude that transient slow slip may promote the conditions required for interactions and clustering, but a variety of interaction mechanisms may be in play (e.g., dynamic or static stress transfer). They showed LFEs to be highly clustered spatially and temporally and interpreted aspects of the clustering as evidence for interactions between LFE sources (measured using a variety of metrics). Importantly, slow slip was accompanied not just by an increase in the rate of LFEs but the degree to which they clustered and interacted with one another, which they showed related to an increased spatial density of critically stressed LFE source patches promoted by surrounding slow slip. In addition, clustered LFEs likely occur in the absence of larger-scale slow slip transients, either because their sources interact as inferred in *Frank et al*. [2016] or by chance as a Poisson process similar to "background" seismicity [*Michael*, 2012].

3. Analytic Clustered LFE Model

In this section, we consider a mathematical model of VLF events represented as a clustered arrival of signals from rapid slip events, evident as a finite series of pulses or LFEs. Figure 2a shows the model proposed (labeled "Model") where a series of LFEs each with time constant τ_c (subscript "*c*" consistent with other publications in which τ_c approximates the inverse of the source "corner" frequency, f_c) are separated by a time τ_s, and the whole sequence has an overall envelope with time constant τ_e. This idealized sequence (labeled Model in Figure 2a) is only an approximation to real sequences of LFEs (labeled "Real" in Figure 2a), which may be envisioned by adding the middle series to the idealized one. We propose that the idealized model predictions capture the key features of a cluster of LFE signal arrivals in the passband of interest; i.e., the variability in LFE features (illustrated by the "Irregularity" time series in Figure 2a) will average to zero, and for reasons described below, artifacts arising from the model's periodicity lie outside this passband. The results of the simulations described in section 4, in which τ_s varies, validate this proposal and are consistent with the predictions of this mathematical model. To illustrate the mathematical model more clearly, we show the case in which the LFE signals do not overlap and $\tau_s > \tau_c$ (top, Figure 2a), and also the case more representative of overlapping LFE signals that manifest as tremor in which $\tau_s < \tau_c$ (bottom, Figure 2a).

Our model includes two functions: $p(t)$, which describes the individual pulse shape (LFE signal), and $e(t)$, which describes the shape of the envelope. In time both functions are nonzero over limited ranges: $p(t) \neq 0$ only if $|t| < \tau_c/2$ and $e(t) \neq 0$ only if $|t| < \tau_e/2$. (We use τ_c to represent the pulse duration because its Fourier

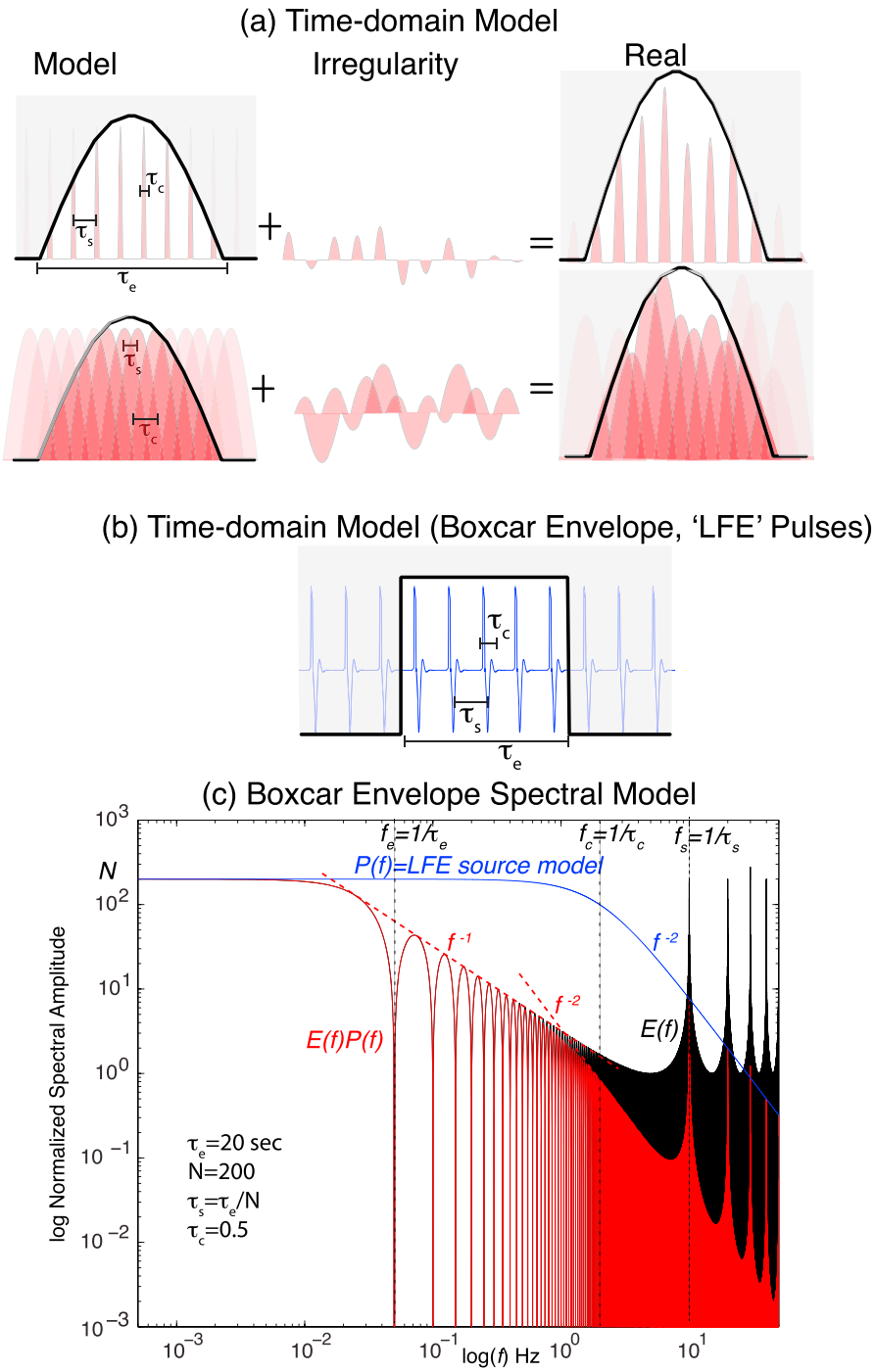

Figure 2. Theoretical model of clustered LFEs. (a) Cartoon of a model of a series of identical pulses (pink) of width, τ_c, arriving at regular intervals, τ_s, and multiplied by an envelope (gray shading, black curve) of width τ_e. The top and bottom panels show the cases in which $\tau_s > \tau_c$ and $\tau_s < \tau_c$, respectively. (b) Specific example of the model in Figure 2a, in which the envelope is a boxcar and the pulses have shapes and spectra similar to those of LFEs. (c) Spectra of an LFE source (blue, $P(f)$), a series of N delta functions (black, $E(f)$), and the windowed series of LFEs (red, $E(f)P(f)$). The spectrum of the windowed LFE series is calculated analytically, for expressions (3), (5), and (6) and parameters noted in the figure. Note that the amplitude of the flat portion of the spectrum is N times that of a single LFE, and the lowest corner frequency and spectral decay below this are determined by the envelope shape and duration. See text for more explanation.

transform will contain a corner frequency f_c). The transient train of pulses in Figure 2a may be described by the expression

$$x(t) = e(t)\sum_{n=-\infty}^{n=\infty} p(t - n\tau_s) \tag{1}$$

where τ_s is the spacing between pulses. This sum of LFE signals may be written more compactly as

$$x(t) \;=\; e(t)[c(t) * p(t)] \tag{2}$$

where $c(t)$ is an infinite train of delta functions (often called a comb function) spaced at intervals τ_s, and the asterisk indicates convolution. In this model many LFE signals arrive in the time span of the envelope function, so $\tau_s << \tau_e$. We denote the spectrum, or Fourier transform of $x(t)$ by $X(f)$, and use the convolution and similarity theorems of Fourier theory to express $X(f)$ as

$$X(f) = \tau_c\tau_s\tau_e P_{f_c}(f)[C_{f_s}(f) * E_{f_e}(f)] = \tau_c\tau_s\tau_e P_{f_c}(f)\sum_{n=-\infty}^{n=\infty} E_{f_e}(f - nf_s) \tag{3}$$

in which $P(f)$, $C(f)$, and $E(f)$ are the Fourier transforms of $p(t)$, $c(t)$ and $e(t)$, and $f_e = 1/\tau_e$, $f_s = 1/\tau_s$, $f_c = 1/\tau_c$.

Expression (3) implies the Fourier transform of the pulse, or, LFE, train is a series of spectral peaks, each with the form $E_{fe}(f)$, that repeat at frequency intervals f_s. The series of peaks is windowed by the Fourier transform of the LFE, $P_{fc}(f)$. As noted above, because the series contains multiple pulses and $f_e << f_s$, the peaks are separated in frequency by more than their bandwidth. The regular spacing of the peaks comes from the assumed uniformity in the spacing of the LFE arrivals, and thus to some degree may be considered an artifact of the model. Moreover, if numerous LFEs arrive within the cluster, or τ_s is sufficiently small, the frequency peaks at $f_s = 1/\tau_s$ and its multiples may be outside the LFE and even the tremor passbands and thus can be neglected, since they would be filtered out by the filtering needed to eliminate microseism and other noise; in most VLF studies band-pass filters are used to retain energy between 0.01 and 0.05 Hz, while in tremor and LFE studies only the 1–10 Hz energy is retained.

To this point, we have not specified the shape of either the LFE signals or the envelope of the cluster, $p(t)$ or $e(t)$, respectively. Regardless of the precise shape of either the formulation above shows that the spectrum of a sum of clustered LFE signals is the product of $P(f)$ and $E(f)$ (equation (3)). Because the time-domain duration and frequency-domain passband always vary inversely, the greater duration of $e(t)$ means it will determine the combined signal's characteristics at the lowest frequencies and likely those in the VLF passband. In other words, the spectral characteristics are determined by the envelope; the envelope may reflect the chance arrival pattern of multiple LFE signals, some more coherent underlying source process or some combination of these. This will be true for any shape LFE or cluster envelope, because of the properties of "pulse-like" functions with a finite area. We show in Appendix A that the Fourier spectrum of any such pulse will have these properties: (1) approach a constant value at small frequencies and (2) decay at high frequencies at a rate f^{-n}, such that the function first becomes discontinuous at the nth time derivative. The spectrum thus has zero- and high-frequency asymptotes that always intersect at a corner frequency approximately equal to the inverse of the pulse width.

In summary, the properties listed in the previous paragraph, and the fact that the envelope is wider than an individual LFE, or $f_e << f_c$, imply that the spectrum will be described by a flat portion for $0 < f < f_e$, a decay rate that depends on the envelope shape for $f_e < f < f_c$, and for $f > f_c$ a decay rate that is further modified by the shape of the LFE. In other words, at frequencies below the LFE corner frequency the spectrum is determined entirely by the envelope, the shape of which is determined by interference pattern of multiple LFE arrivals. The mathematical model in this section shows all this to be true analytically. While this requires the assumption of regular intervals between LFE signals, the resulting artifacts lie outside the passband of interest. Moreover, the simulations presented in section 4 verify that these properties apply even when the intervals are highly variable.

We illustrate this theoretical model for a boxcar envelope, chosen because it is simple and yields an analytic form for $X(f)$. Following *Hotovec et al.* [2013] (Appendix A), the Fourier transform of a Comb function is the series

$$C\left(\frac{f}{f_s}\right) = \sum_{n=-\infty}^{\infty} \exp\left(-i2\pi n\frac{f}{f_s}\right) \tag{4}$$

The convolution of this with a boxcar that spans N LFE signals is equivalent to truncating the series after N terms (Figure 2b). This finite sum has the analytic form

$$C\left(\frac{f}{f_s}\right)*E\left(\frac{f}{f_e}\right) = e^{\left(-i2\pi\frac{f}{f_s}\right)}N\frac{\mathrm{sinc}\left(\pi\frac{f}{f_e}\right)}{\mathrm{sinc}\left(\pi\frac{f}{f_s}\right)} \tag{5}$$

In Figure 2c we show an example of a spectrum $X(f)$ calculated according to expression (5) and a Brune source model [*Brune,* 1970, 1971], or

$$P\left(\frac{f}{f_s}\right) = M_0\frac{1}{\left[1+\left(\frac{f}{f_c}\right)^2\right]} \tag{6}$$

We use parameters appropriate to those in real observations, i.e., a cluster duration $\tau_e = 20$ s, $N = 200$, $\tau_s = \tau_e/N = 0.1$ s, and $\tau_c = 0.5$ s or $f_c = 2$ Hz [*Bostock et al*., 2015]. Note that when $\tau_s < \tau_c$, corresponding to LFE signals that overlap significantly, as they would during bursts of tremor, the harmonics would occur above the VLF and tremor passbands (red curve, Figure 2c). Moreover, the harmonics arise because of the periodicity assumed in order to derive an analytic model and thus may be considered to be artifacts. As noted above, the simulations with variable τ_s described in section 4 demonstrate this, and that the precise spacing of the LFE signal arrivals is unimportant as long as $\tau_s < \tau_c$. As predicted, the spectrum has a shape that largely reflects that of the envelope of the clustered LFEs, with a lower corner frequency approximately equal to the inverse of the envelope duration and a higher corner equal to that of the component LFE. While a boxcar is an overly simplified representation of real envelopes, which will vary from one LFE or tremor cluster to the next, we suggest it is a reasonable, first-order representation. Interestingly, the spectrum decays as f^{-1} between about 0.02 and 2.0 Hz, as observed in several studies of VLF, LFE, and tremor seismic signals.

In conclusion, regardless of the specific shape of the LFE or tremor source spectra, or of the envelope of a burst of arriving signals, the low-frequency attributes of the composite spectrum will reflect the characteristics of the latter. If one applies a narrow band-pass filter to remove all energy outside this low-frequency passband (as is often done to eliminate noise), there is then no way to tell the difference between a sequence of brief pulses (LFEs and tremor) spread over a longer time and a single pulse (VLF source) acting over the same time. The corner frequency observed might thus be associated not with the time during which a larger source slips but with the time over which a sequence of smaller, similar events occurs in a kind of miniswarm or simply arrive nearly simultaneously by chance. Additionally, the spectral decay rate of such a band-passed signal also may reflect only the manner in which a burst of multiple signals arrives in a short window, rather than the slip speed of a single slow source.

4. Synthetic VLF Events

In this section, we construct synthetic, idealized LFE signal clusters to test the idea that VLF events are just clusters of independent LFEs, rather than slow earthquakes resulting from a coherent slip event that is several orders of magnitude larger. Use of synthetics rather than real-LFE signals has the benefit of avoiding the low-frequency noise that often obscures signals with periods of tens of seconds or more [*Agnew and Berger*, 1978; *Berger et al*., 2004; *Barbour and Agnew*, 2012]. We attempted to simulate VLF events using those of real LFEs but found that the low-frequency noise masked the signal in the VLF passband. To be sure that the low-frequency energy in the summed signal was noise, we computed ratios of individual LFE waveforms in a single family and the family's "template" LFE, and then stacked these ratios. The family's template should be nearly noise free (W. Frank, personal communication, 2015) so that the ratio should remove the effect of coherent signals with any deviation from one representing incoherent noise. The noise at frequencies above the microseism peak did appear to cancel when the ratios were stacked, evident as ratios equal to one, but did not at lower frequencies. We suspect that this is because destructive interference of noise by stacking requires noise to be stationary (its mean amplitude and standard deviation are invariant), which likely is not the case; although we did not test this rigorously, we suspect that occasionally the low-frequency noise becomes extremely large and dominates the stack.

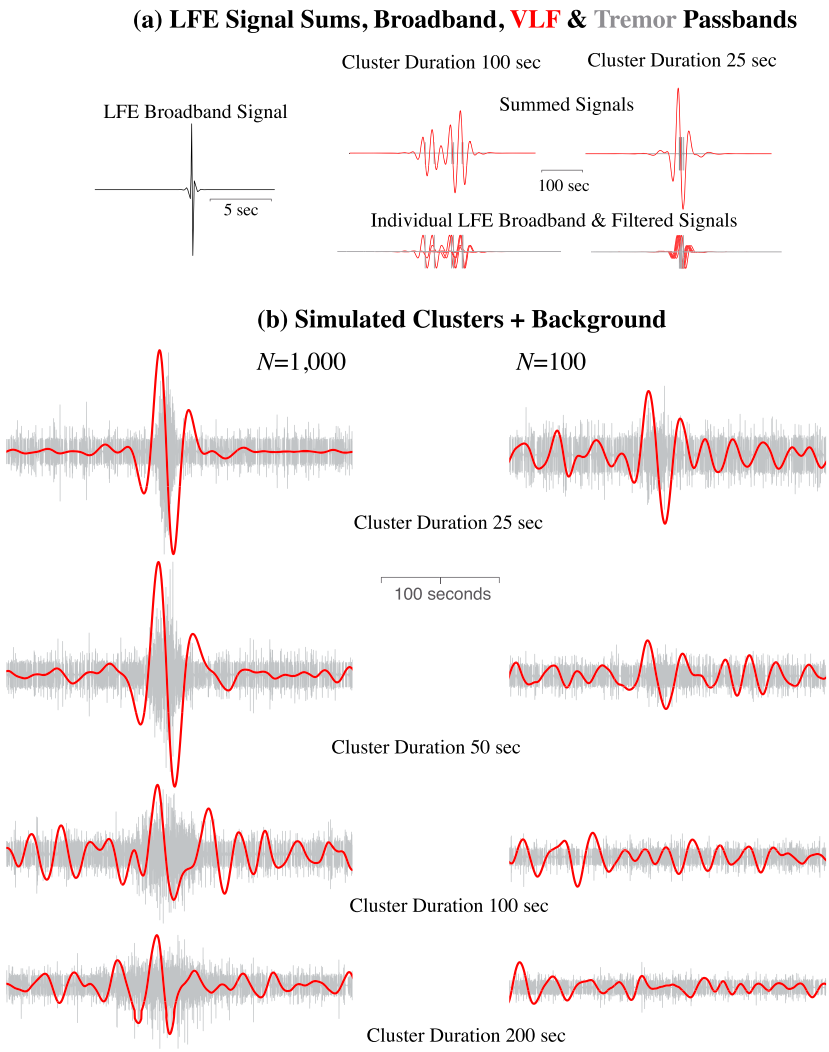

Figure 3. Simulated LFE cluster, in tremor and VLF passbands. (a) Schematic showing how the duration of a cluster of LFE signals affects the coherent summing of low-frequency components. Six copies of a simulated broadband velocity waveform (pulse on left) that have been band-pass filtered in the tremor (2–8 Hz, gray) and VLF (0.02–0.05 Hz, red) passbands are distributed with random offsets. When filtered pulses are spread over 50 s (lower right) and they sum to form a pulse (upper right). When spread over 200 s (lower center) the pulse-like character of the sum diminishes (upper center). (b) Sum of $N = 100$ (right) and $N = 1000$ (left) of the filtered LFE signals in Figure 3a with arrival times sampled randomly from a normal distribution spread over the durations labeled and added to a background of 655 s containing LFES signals at 2000 uniformly distributed random times.

We simulate a velocity seismogram of an LFE by differentiating a delta function and low-pass filtering it with a corner frequency at $f_c = 3$ Hz and a high-frequency spectral decay rate of f^{-2}. A zero-phase, first-order Butterworth filter accomplishes this. We choose 3 Hz to be consistent with measured values for LFEs in Cascadia ($f_c \sim 2$–3 Hz [*Bostock et al.*, 2015]) and Parkfield, California ($f_c \sim 5$ Hz [*Thomas et al.*, 2016]). Such a spectrum is consistent with an "omega-squared" or "Brune" earthquake source model [*Brune*, 1970, 1971] and may appropriately represent the source spectrum of LFEs [*Zhang et al.*, 2011]. As illustrated schematically in Figure 3a using only six (for clarity) of these synthetic LFE signals, when these signals arrive within an interval comparable or less than the dominant period of the passband of interest for VLF events (~20–50 s period or ~ 0.02–0.05 Hz) and are filtered in this passband, the filtered waveforms add constructively when summed and a low-frequency pulse results (right example, Figure 3a). A zero-phase filter produces a pulse centered on the peak of the cluster (we use a second-order Butterworth filter). Comparison of the with summed signals spread over a longer duration shows that such constructive interference and pulse-like waveforms diminish or disappear as filtered arrivals overlap by lesser amounts or not at all (left example, Figure 3a). We test this

more rigorously by generating a cluster of LFE signals or, equivalently a tremor burst, by summing N identical synthetic LFE signals that are time shifted with normally distributed random arrival times. We spread the arrivals of N LFEs over an interval that corresponds to an approximate tremor burst with duration, D, which is approximately equal to an interval of -3σ to $+3\sigma$ in which σ is the standard deviation of the distribution of arrival times (i.e., 99.7% of the N LFE signals arrive within the interval D).

Figure 3b shows the results of band-pass filtering simulated clusters of $N = 100$ and $N = 1000$ LFE signals for different cluster durations, chosen to be similar to those in *Ide et al.* [2008] (see their Figures 3 and 4). To make these more realistic, we have also added a background of 2000 LFE signals that arrive at uniform randomly distributed times over an interval of 655 s. The results confirm the expectations described above and from the analytic model in section 3 (but now without the regularity in LFE signal arrival times). Figure 3b shows that when the cluster duration is comparable to the period range of the passband, even a cluster of 100 LFEs produces a pulse-like signal when filtered in that passband and in the presence of background activity that is only slightly smaller than the cluster (i.e., the background rate of LFE signal arrivals is ~3/s while that for the cluster is ~4/s). As the cluster duration spreads and/or it contains fewer arrivals, the apparent VLF event diminishes.

The characteristics of the VLF pulse that emerge from band-pass filtering a clustered sum of LFEs, or a tremor burst, plausibly explains all the features of observed VLF events. These features include (1) estimated magnitudes that are several orders of magnitude larger than those of LFEs [*Ide et al.*, 2008], (2) depletion in high frequencies relative to an earthquake with comparable low-frequency spectral amplitude [*Ito et al.*, 2009; *Takeo et al.*, 2010], (3) spectral decay rates of $\sim f^{-1}$ [*Ide et al.*, 2007a], (4) waveforms that may be fit with moment tensors consistent with the tectonic loading [*Ito and Obara*, 2006b; *Ide et al.*, 2008; *Ito et al.*, 2009], and (5) source locations shared with those of tremor and LFE sources [*Ito and Obara*, 2006a; *Takeo et al.*, 2010; *Walter et al.*, 2013]. We demonstrate the consistency of these features with VLF waveforms that arise from summed LFE signals in the examples that follow.

4.1. Synthetic VLF and LFE Magnitudes

The characteristics of the VLF events derived from a cluster of N LFE signals constructed as described above are predictable. We first demonstrate how they explain the first VLF feature noted above, which estimated VLF amplitudes are several orders of magnitude larger than those of LFEs [*Ide et al.*, 2008]. Each panel of Figure 4 shows the results for 20 individual simulations and their average, for cluster durations that vary by 20% around the same durations as in Figure 3 (25, 50, 100, and 200 s) but without the background LFEs. The more clustered the LFEs are (the shorter the specified duration), the more coherently the low-frequency spectral components add so that the summed VLF pulse amplitude grows (note the different waveform amplitude scales in Figure 4) and the low-frequency spectral amplitude approaches a value that is N times greater than that of the LFE (Figure 4, bottom row). However, the higher-frequency components sum incoherently and if truly random, the summed spectral amplitudes will be $N^{1/2}$ times as large as those of an individual LFE signal. In summary, the spectrum of N summed clustered LFE signals will have a low-frequency spectral level approximately equal to that of a VLF with $M_0{}^{\mathrm{VLF}} = N\, M_0{}^{\mathrm{LFE}}$ and high-frequency spectral level equal to $N^{1/2} M_0{}^{\mathrm{LFE}}$ beyond the corner frequency of the LFE (Figure 4a, bottom row). We note that the increase by a factor of N at low frequencies agrees with the analytic model presented in section 3.

We estimate the number of LFEs that must be summed to generate a VLF that is ΔM_w moment magnitude units greater than the LFE's magnitude, and how the areas of N LFEs might compare with that of a driving slow slip event or SSE (Figure 1b, top). From the definition of moment magnitude, $N = 10^{\alpha M}$ with $\alpha = 1.5\Delta M$. For example, the cases in Figures 3 and 4 with $N = 1000$ LFE signals give rise to estimated VLF magnitudes 2.0 units larger than that of the LFE. If LFEs represent small, strong spots within surrounding slowly slipping regions, then we need to ask if N LFEs may fit within such regions. The ratio of the areas of N LFEs to that of a driving slow slip event may be estimated assuming the source areas of both may be calculated as

$$A = (M_0/k\Delta\tau)^{2/3} \tag{7}$$

in which M_0 is seismic moment, k is a constant ~1, and $\Delta\tau$ is stress drop [*Aki*, 1972]. Thus, the ratio of the areas of N nonoverlapping LFEs to that of an SSE is $N(M_0{}^{\mathrm{LFE}}/M_0{}^{\mathrm{SSE}})^{2/3}(\Delta\tau^{\mathrm{SSE}}/\Delta\tau^{\mathrm{LFE}})^{2/3}$. This ratio of LFE to SSE area plausibly could be less than one, noting that the moments associated with the cumulative tremor or LFEs associated with an accompanying SSE typically are orders of magnitude smaller [*Kao et al.*, 2010; *Ochi and*

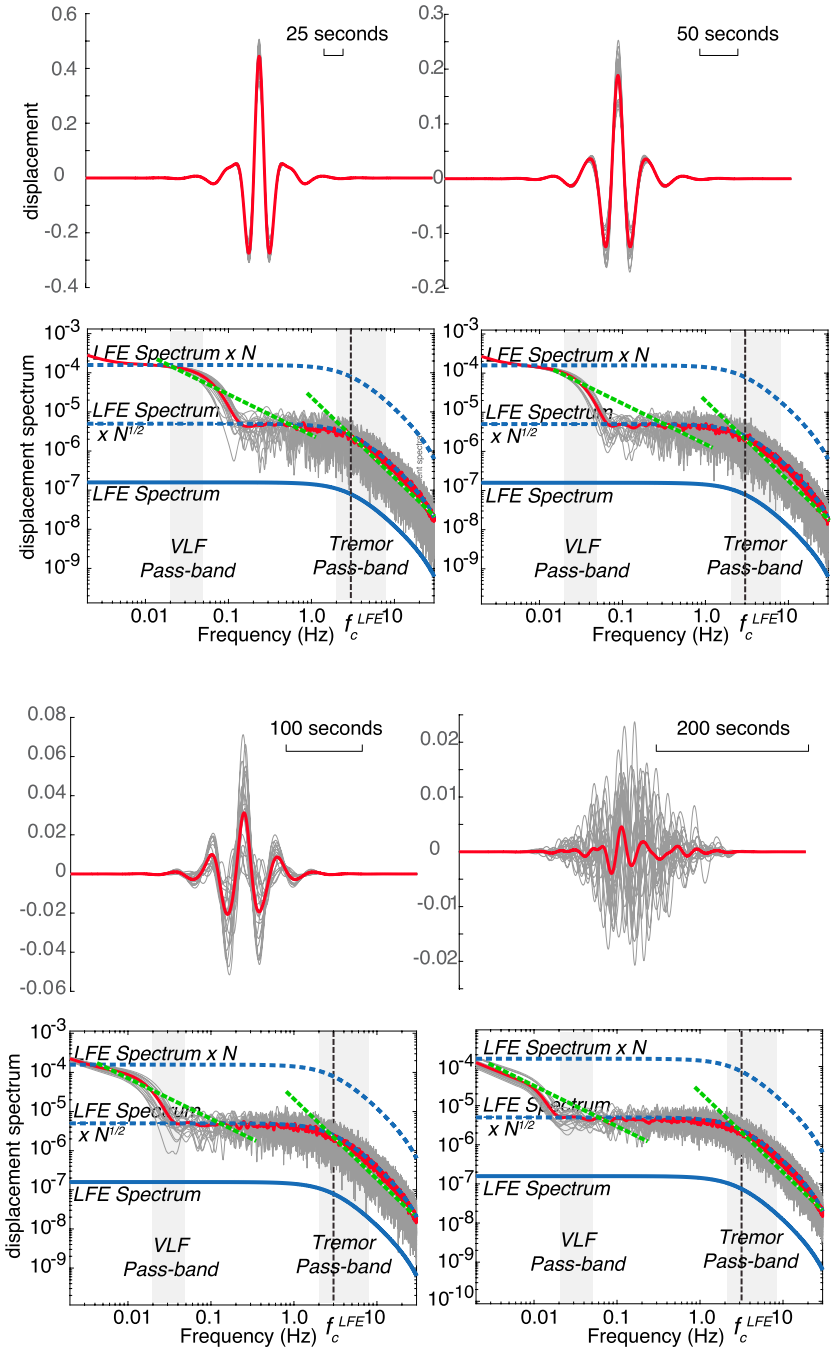

Figure 4. Effect of LFE cluster duration and variability on VLF waveforms. For each duration, we show 20 realizations of simulated displacement (top) waveforms and (bottom) spectra and their averages in gray and red, respectively. Absolute amplitude units are arbitrary but the same for all simulations. In each realization $N = 1000$ identical LFE signals (Figure 3a) were summed and the sum band-pass filtered between 0.02 and 0.05 Hz (see text). Spectra of the LFE alone and multiplied by N and $N^{1/2}$ are shown in solid and dashed blue lines, respectively, and green dashed lines indicate spectral decay rates of f^{-1} and f^{-2}. Cluster durations are labeled and shown with scale bars.

Kato, 2013]. Additionally, if LFE source areas overlapped, this effectively reduces N. Finally, while estimation of stress drops of LFEs are highly uncertain because the slip and areas can only be inferred very indirectly [*Sweet et al.*, 2014; *Bostock et al.*, 2015], the ratio of SSE to LFE stress drops most likely is <1; e.g., *Sweet et al.* [2014] estimate $\Delta\tau^{\mathrm{LFE}}$ could be between a few kPa to several MPa. Typically, when measured geodetically $\Delta\tau^{\mathrm{SSE}}$ estimates are more well constrained, with values in the range of ~10–100 kPa [*Gao et al.*, 2012].

4.2. Synthetic VLF and LFE High-Frequency Depletion

The second VLF feature to explain is the VLF depletion in high frequencies relative to an earthquake with comparable low-frequency spectral amplitude [*Ito et al*., 2009; *Takeo et al*., 2010]. As noted above and illustrated in Figure 4, the apparent moment of the VLF event, or cluster of LFEs, is $M_0{}^{\mathrm{VLF}} = NM_0{}^{\mathrm{LFE}}$ and the corner frequency, f_c, of LFE cluster is the same as that for a single LFE signal, $f_c{}^{\mathrm{LFE}}$. We relate f_c to M_0 using the definitions for stress drop (equation (7)) and corner frequency, f_c,

$$f_c = \left({}^{2.34V}/_{2\pi}\right)\left({}^{k\Delta\tau}/_{M_0}\right)^{1/3} \tag{8}$$

with V denoting rupture velocity. To guarantee that the apparent VLF is depleted in high frequencies relative to an earthquake with the same moment, or $M_0{}^{\mathrm{eq}} = NM_0{}^{\mathrm{LFE}}$, requires that $f_c{}^{\mathrm{eq}} > f_c{}^{\mathrm{LFE}}$, with superscript eq referring to earthquake values. Assuming similar rupture velocities for the LFE and earthquake (both must be close to the shear velocity to be seismic), this requirement implies

$$\left({}^{\Delta\tau^{\mathrm{eq}}}/_{M_0{}^{\mathrm{eq}}}\right)^{1/3} > \left({}^{\Delta\tau^{LFE}}/_{M_0{}^{\mathrm{LFE}}}\right)^{1/3} \quad \text{or} \quad \Delta\tau^{\mathrm{eq}} > N\Delta\tau^{\mathrm{LFE}} \tag{9}$$

Bostock et al. [2015], *Sweet et al*. [2014], and *Thomas et al*. [2016] have estimated $\Delta\tau$ for LFE signals, and *Shelly et al*. [2007] showed stacks of spectra for LFEs, earthquakes, and tremor (their Figure 2). Results of these studies indicate LFE corner frequencies, and inferred $\Delta\tau$ values are less than those for earthquakes of comparable magnitudes by several orders of magnitude. Estimates of $\Delta\tau$ by *Brodsky and Mori* [2007] for large "tsunami" (slow rupturing) earthquakes do not differ significantly from faster earthquakes, but those for relatively aseismic creep events lasting days or longer are lower by an order of magnitude or more. *Fletcher and McGarr* [2011] estimated that $\Delta\tau$ for tremor events were more than an order of magnitude smaller than those of earthquakes, and in their analysis of VLF *P* waves *Ito and Obara* [2006b] concluded that their $\Delta\tau$ values were 2–3 orders of magnitude smaller than the range for earthquakes of comparable moment. These studies and our synthetic examples suggest the requirement of equation (9) may be satisfied.

4.3. Synthetic VLF and LFE Spectral Decay Rate

The third feature to explain is the spectral decay rate of $\sim f^{-1}$. Figure 4 shows the spectra of summed LFEs for four different cluster durations. At frequencies above the VLF passband, the spectral components add randomly and the spectrum is simply a scaled version of the LFE spectrum, by a factor of $N^{1/2}$. At lower frequencies the spectrum of the cluster envelope dominates and approaches a level N times that of an individual LFE signal. These $N^{1/2}$-fold and N-fold increases are expected for signals that add randomly and coherently, respectively, noting that as the cluster duration decreases the low-frequency spectral components add more constructively and the spectrum becomes flatter. The addition of noise and some variability in the component LFEs would likely smooth these idealized spectra, yielding spectra that may decay as f^{-1} from the lowest measurable frequency to approximately $f_c{}^{\mathrm{LFE}}$. Even if not describable precisely as f^{-1}, these examples show that the decay rate will be slower than the f^{-2} that typifies earthquakes. Although not shown, if the LFE spectral decay rate is close to f^{-1} instead of f^{-2} as assumed in the example, the summed LFE signal would decay as f^{-1} or slower for the entire spectrum.

4.4. Synthetic VLF and LFE Moment Tensors

Finally, we consider the similarity between moment tensors and hypocenters estimated from VLF, LFE, and tremor signals (fourth and fifth features). Synthetic tests show that the shape of the VLF pulse is a longer period version of the LFE waveform and does not change significantly when the cluster duration varies by $\pm$20%. Thus, if the LFEs and tremor (assumed to be composed of LFEs) are consistent with tectonically sensible moment tensors or hypocenters, the band-passed signal derived from a cluster of randomly summed LFEs also will be. Hypocenter estimates are constrained primarily by the move-out patterns of the arrival times of VLF centroids, so that as long as the clustering of the component LFEs does not vary significantly across the network, the move-out pattern and hypocenter estimates also should be very similar to that of the centroid of the LFE distribution.

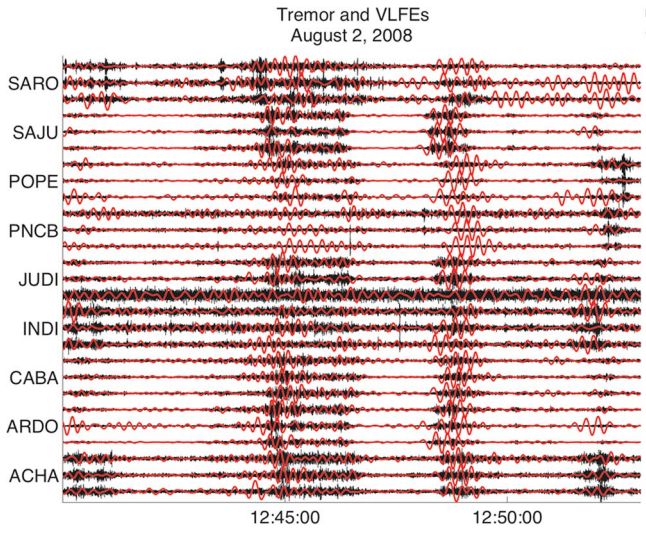

Figure 5. Example of amplitude normalized very low frequency events (12–30 s band-pass filtered) embedded within higher-frequency (2–8 Hz band-pass filtered) tremor during the August 2008 northern Costa Rica slow slip event.

5. Observational Evidence From Costa Rica

Support for VLF events representing a single, coherent slip event would be given by observations of them when smaller slip events were not occurring, i.e., in the absence of active tremor or LFE. Although a failure to find VLF events without concurrent tremor or LFE clusters does not rule out the possibility of a single, larger coherent slip event, it does support our proposal that interpretation of VLF events is nonunique. Here we describe observations from the northern Costa Rica subduction zone during several 5–14 day shallow slow slip events that show VLF events only occurring during tremor episodes and never as isolated events. Tests comparing spectral amplitudes of tremor and VLF events to those predicted by our analytic model and simulations would be useful but are beyond the scope of this study.

The seismogenic zone beneath the Nicoya Peninsula, Costa Rica, exhibits diverse slip behavior including normal earthquakes, slow slip, tremor, low, and very low frequency earthquakes. During the last 163 years, four large megathrust earthquakes occurred beneath the Nicoya Peninsula: 1853, 1900, 1950 (M_w7.7), and 2012 (M_w7.6) [*Protti*, 2014]. Since 2003 GPS and seismic networks on the Nicoya Peninsula have recorded 10 slow slip events accompanied by tremor [*Outerbridge et al*., 2010; *Walter et al*., 2011; *Jiang et al*., 2012; *Dixon et al*., 2014]. Large slow slip events repeat every 21 ± 6 months, with smaller events occurring much more frequently [*Jiang et al*., 2012; *Dixon et al*., 2014]. All of the SSEs are accompanied by tremor with both LFE and VLF events detected within this tremor [*Brown et al*., 2009; *Walter et al*., 2013]. Tremor is routinely located using envelope cross-correlation methods and, in general, is poorly located.

Walter et al. [2013] documented the synchronous occurrence of geodetically detected slow slip, tremor, and VLF events at shallow depth offshore the Nicoya Peninsula in August 2008. During the first week of August 2008, they identified 54 VLF events. Figure 5 shows 15 min of seismic data during this time period illustrating the VLF events embedded within the tremor. The temporal overlap between the tremor bursts and VLF events is a ubiquitous characteristic.

We used the events in the *Walter et al*. [2013] VLF catalog as candidate template events and applied a matched-filter technique to identify additional VLF events during this and three other slow slip episodes. VLF events with high signal-to-noise ratios at 5 or more, three-component stations were retained as template events. The periods of time investigated had both geodetically determined slow slip and abundant tremor and included 16–22 May 2007, 31 July to 7 August 2008, 1–10 March and 20–27 June 2009, and 8–26 October 2010. For all intervals, continuous velocity time series were filtered between 12 and 30 s and downsampled to 1 Hz. The technique computes the cross-correlation values between the template event and continuous data at each sample point to obtain a cross-correlation function (CCF). The CCFs for all stations and components are then stacked to produce a single summed CCF. Detection occurs when the summed CCF exceeds a threshold value similar to other studies utilizing a network-based matched filter [*Shelly et al*., 2007]. An example of the summed CCF, positive event detections and VLF waveforms for a 2008 template and its matches are shown in Figure 6.

We identified VLF events that repeated over multiple SSE episodes by cross correlating the templates identified in 2008, and their highest quality matches, and selecting all time periods with summed CCFs that exceeded our threshold. In total we have detected over 100 VLF events using five different template events.

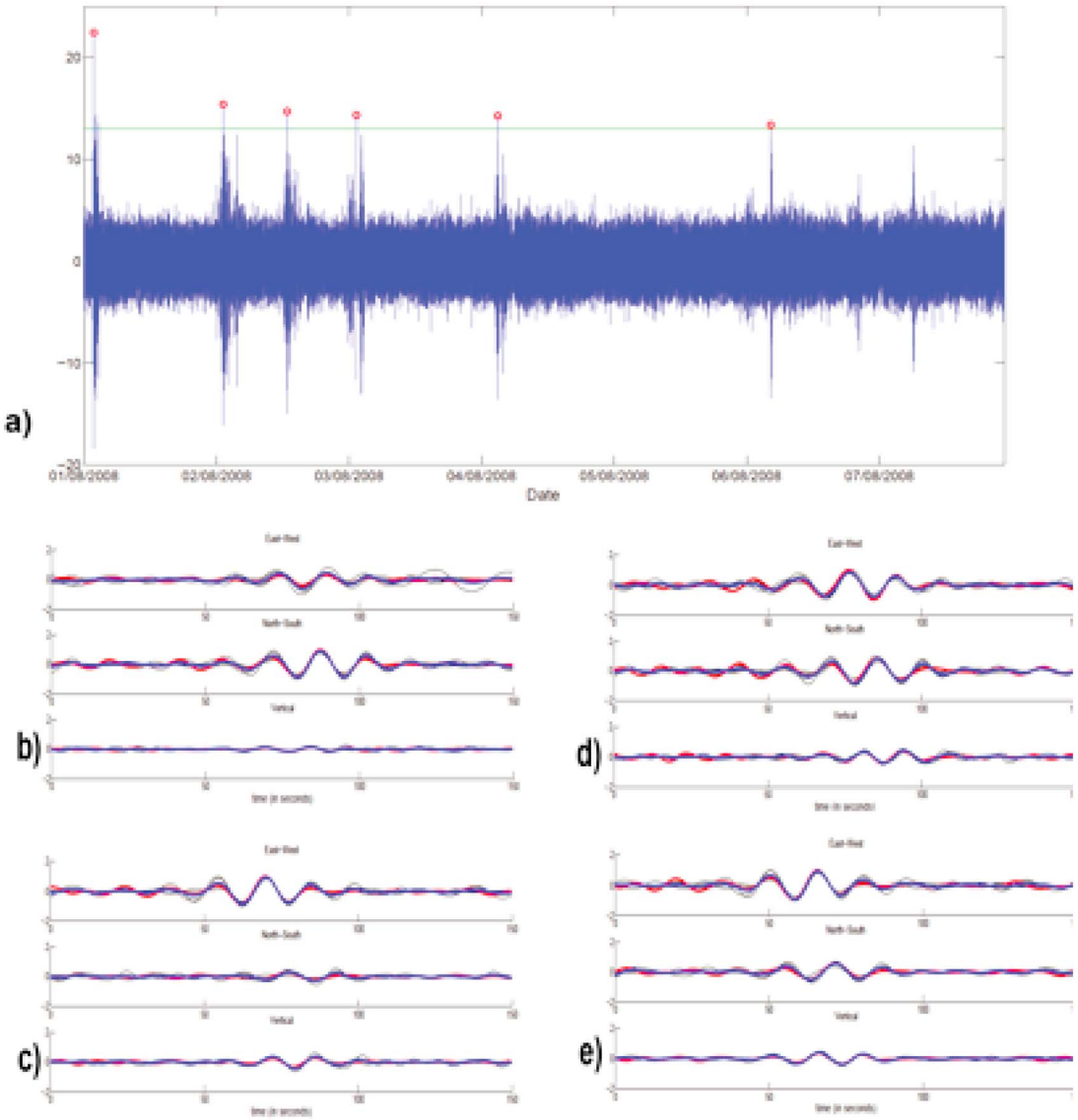

Figure 6. (a) Result of the cross correlation (blue trace) between a template VLF in 2008 and 7 days of data (filtered in the passband 12–30 s). The highest peak corresponds to the cross correlation of the template with itself. The smaller peaks above the threshold (green line) correspond to matches. (b–e) Waveform comparisons for stations ACHA, ARDO, CABA, and SAJU, respectively, between the template (red trace), the five matches (black traces), and the stack of all the matches in this time interval (blue trace). For each event, all trace amplitudes are normalized to the peak value at that station.

An example of a high quality template event and the matches it identifies through the entire time period (excerpts of 2007–2010) is shown in Figure 7. Each template identifies positive detections during all slow slip events that show remarkable waveform similarity, leading us to conclude that discrete patches of the fault plane are consistently reactivated during subsequent SSE episodes. The dimensions of these patches cannot be resolved but are likely within several tens of kilometers, which is the location uncertainty of some of the VLF sources. If VLF events are composed of signals from multiple LFE sources, then they may be separated by comparable distances. We also visually identified several VLF events that were distinct from the original templates and cross correlated them through the time period of interest. These templates also yielded many matches, revealing the existence of distinct template families.

Application of this matched-filter search to all 4 years of continuous data is beyond the scope of this study; however, our finding that all VLF detections are synchronous with tremor (2–8 Hz), which itself occurs less than 10% of the time (~90 h of 1248 h analyzed), supports the hypothesis that VLF events represent a superposition of LFE arrivals observed through a low-pass filter. These VLF events, as well as the tremor they are

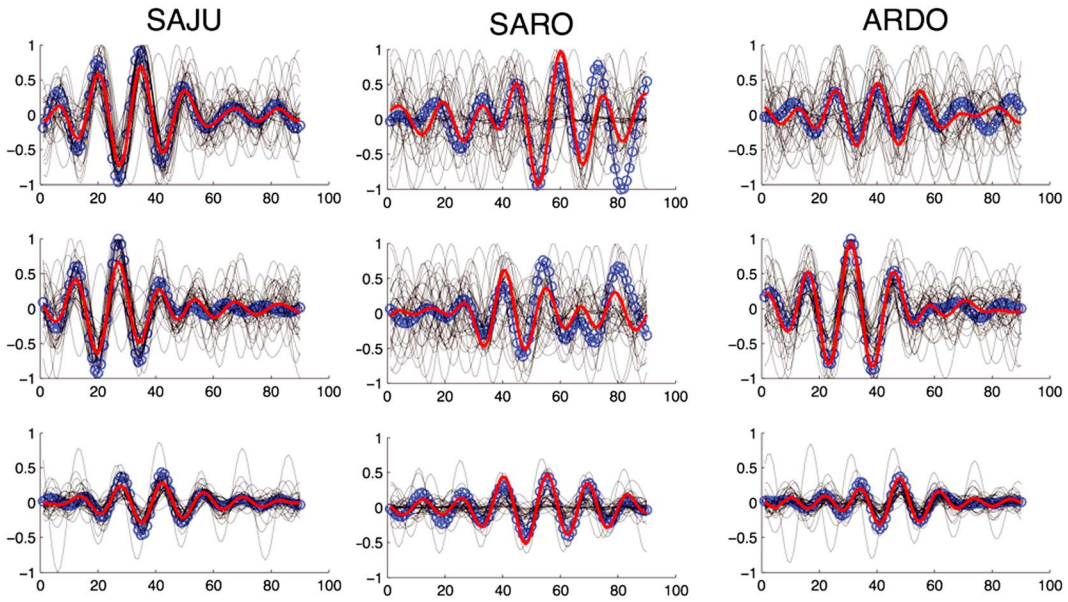

Figure 7. The 9 October 2010 template and matching velocity waveforms for three stations. Similarity between the template event (red trace), the matches (black traces), and the stack of all waveforms (blue trace) is excellent even though waveforms span the time period between 2007 and 2010. All three-component (top row: east, middle row: north, and bottom row: vertical) data are normalized by station.

embedded within, are located by cross-correlating envelopes in both the low- and high-frequency bands. VLF events detected with templates from different families yield distinct source locations (different by >25 km), while synchronous VLF and tremor, regardless of their template family, always produce indistinguishable locations considering their uncertainties of as much as 20 km.

6. Discussion and Conclusions

Although VLF pulses produced by band-pass filtering a clustered sum of LFEs share characteristics with observed VLF events, this does not rule out the possibility that some VLF events may originate from single, much larger coherent slow earthquakes. However, the ubiquitous simultaneity of VLF with tremor and LFE signals, particularly during tremor bursts, suggests that many VLF events could be clusters of independently rupturing and radiating LFEs. We have used theoretical and synthetic models to show that a cluster of LFE signals or tremor produces the characteristics of VLF events, and, most importantly, that the key VLF attributes used to infer source characteristics may instead arise from the envelope or shape of the cluster. While a VLF event may be radiated from transient slow slip that propagates coherently and quasi-dynamically over dimensions of tens of kilometers, it also may result from a superposition of signals from slip on numerous smaller patches with dimensions of tens of meters that rupture at higher velocities. These latter LFEs may be triggered by a single aseismic slow slip front propagating coherently over tens of kilometers or by spatially and mechanically distinct but nearly simultaneous smaller aseismic slip events. Additionally, as in regular earthquakes and aftershocks, clusters of LFEs may arise because they interact with one another (e.g., via dynamic or static stress transfer) or possibly even by chance superposition of multiple background LFEs that fail due to constant tectonic loading. In the interpretation of a VLF event as a single, dynamic slip event we would expect that VLF events would occasionally be observed without accompanying higher-frequency tremor or LFE signals. While not proving the alternative interpretations, analyses of continuous data from Costa Rica recorded over periods of 8 to 20 days each in the years 2007 through 2010 yielded no detections of VLF events in the absence of tremor. Although tremor occurred during less than 10% of these periods, matched-filter template scanning through all these data detected VLF events only concurrent with the tremor.

We suggest that the VLF observations may be interpreted in terms of three end-member source models. These have different implications for the scaling of slip events with size and slip mode, from fast earthquakes

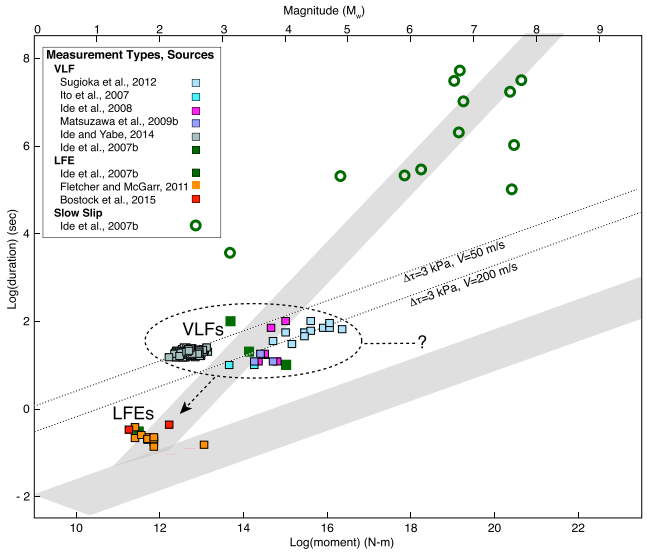

Figure 8. Slip event scalar moment, M_0, versus duration, T, observations and scaling relationships. Inferred slow and fast (steeper and shallower gray bands, respectively) scaling relations are shown with seismic and geodetic measurements (solid and open dark green squares and circles, respectively) of slow slip events reported in *Ide et al.* [2007b]. Published VLF and LFE measurements are shown as squares, with colors assigned to the study each reported in the legend. Dotted lines through the VLF events correspond to fast slip scaling calculated for stress drop and rupture velocities estimated for VLF events [*Matsuzawa et al*., 2009].

to slow effectively aseismic transient slip. We discuss scaling in the context of inferred M_0 versus event duration, T, proposed initially in *Schwartz and Rokosky* [2007] and *Ide et al*. [2007b, 2008].

The first interpretation considers VLF events to originate from M_w2 to 5 slow seismic sources that scale with M_0 proportional to T [*Schwartz and Rokosky*, 2007; *Ide et al*., 2007b, 2008] (steeper gray band in Figure 8). In their interpretation M_0 versus T scaling differs for "slow" and "fast" slip events, reflecting fundamentally different source processes. We note that even these authors acknowledge inconsistencies between slow scaling and VLF measurements. For example, *Ide et al*. [2008] measured M_0 proportional to $T^{3/2}$ but dismissed this deviation from the conventional scaling as an "artifact of the limited frequency range of our analysis, 0.005–0.05 Hz." Later *Ide* [2008] suggested M_0 is proportional to T^2 and proposed a different physical model than that in *Ide et al*. [2007b]. We also note that the same inference offered by *Zhang et al*. [2011] to explain tremor spectra may also apply to VLF measurements, that they scale like regular earthquakes but have lower stress drops and/or slower, but still seismic, rupture propagation velocities (e.g., dotted lines in Figure 8).

The model proposed by *Ide* [2008] appears to fit in this first class and highlights the nonuniqueness in interpreting the VLF and LFE observations. In this model, VLF events represent radiation from transient coherent slip from slip events for which the M_0 versus T scaling differs from earthquakes. For each event, the slipping region is assumed to grow overall, but with "random expansion and contraction" according to an autoregressive model; the resulting fluctuations in moment rate give rise to tremor. *Ide* [2008] noted that the noise-free version of this model does not predict the occurrence of LFE signals as observed, instead predicting durations orders of magnitude longer. *Ide* [2008] suggests that LFE scaling results from only observing radiated energy above the noise threshold, which has a briefer duration. So in this model VLF events would be directly caused by the slip, with the LFE signals being a second-order byproduct: nearly the opposite of our interpretation.

The second and third interpretations consider VLF events to result from the clustered arrival of LFE or tremor signals but clustered for two different reasons. In the second interpretation, the LFE sources result from passage of a slow, effectively aseismic, slip front passing across a fault containing the tiny seismogenic asperities that fail and efficiently radiate seismic waves, much like swarms and aftershocks driven by spontaneous slow slip and afterslip, or as in the laboratory as acoustic emissions that accompany slow preslip [*McLaskey and Lockner*, 2014]. Thus, in this interpretation VLF events serve as proxies indicative of causative, much larger, slower moment release and provide only a lower bound on its magnitude (Figure 8, dashed horizontal line and question mark). However, as in aftershock sequences, *Frank et al*. [2016] note that in some regions clustering of LFEs does not simply reflect the speedup of LFE failure rates as slow slip fronts pass, but the latter actually enhances mechanisms by which LFE patches interact with one another (e.g., via static or dynamic stress transfer). Thus, while associated with larger-scale slow slip, other processes may be important in controlling LFE clustering.

The third end-member interpretation is that the clustering of LFEs need not result directly from a spatially or temporally coherent process like a driving, slower slip transient, but rather may be more like the clustering

that appears in more standard earthquake seismicity as part of the variability inherent in a Poisson process [*Michael*, 2012]. Results shown in *Frank et al.* [2016] may corroborate this as they note that clustered LFEs occur both during and between times of slow slip events in southern Mexico. While they showed that time series of the recurrence intervals of many individual LFEs are non-Poissonian, their observations do show that temporally and spatially clustered LFEs occur in the absence of geodetically detectable slow slip. In this case the VLF moment-duration observations serve only as proxies for LFEs (diagonal dashed arrow in Figure 8). Given all these alternatives, we conclude that VLF events do not provide discriminants between M_0 and T scaling models.

Appendix A

We show here that the Fourier spectrum of a time-limited, finite area pulse will have these properties: (1) approach a constant value at small frequencies, (2) decay at high frequencies at a rate f^{-n}, such that the function first becomes discontinuous at the nth time derivative, and (3) have zero- and high-frequency asymptotes that always intersect at a corner frequency approximately equal to the inverse of the pulse width. The first property arises from the definition of the Fourier integral, which at zero frequency is just the integral over the function, and so is nonzero if the function has a finite area. To first order this area will be A, where A is the amplitude and τ the time constant, and if we take $X(f)$ to be this up to a corner frequency f_c, then $f_c = \tau$. The second fact arises by noting that when the $(n-1)$th derivative of $x(t)$ has a discontinuity, the nth derivative of the discontinuity is a delta function, so that if there are D discontinuities at t_d, $d = 1,\ldots, D$.

$$\begin{aligned}\frac{d^n x(t)}{dt^n} &= \sum_{d=1}^{D}\delta(t-t_d) \quad t = t_d \\ &= \frac{d^n x(t)}{dt^n} \qquad t \neq t_d\end{aligned} \tag{A.1}$$

Since the Fourier transforms of a time derivative of a function equals the product of the function's spectrum and $2\pi if$, and that of a delta function equals one, $X(f)$ may be written

$$X(f) = (2\pi if)^{-n}\frac{d^n X(f)}{dt^n} = (2\pi if)^{-n}\left[\sum_{d=1}^{D} e^{-2\pi if t_d} + \frac{d^n X(f)}{dt^n}\right] \tag{A.2}$$

The contribution of the discontinuities is constant and thus dominates over that of the derivatives at high frequencies, so that to first order

$$|X(f)| \approx (2\pi if)^{-n}\left[1 + 2\frac{d^n X(f)}{dt^n} = (2\pi if)^{-n}\right] \tag{A.3}$$

Acknowledgments
The authors thank Amanda Thomas, David Shelly, Honn Kao, and two anonymous reviewers for their helpful reviews and comments. Seismic data from Costa Rica can be obtained through the IRIS DMC (Nicoya Network code YZ).

References

Agnew, D. C., and J. Berger (1978), Vertical seismic noise at very low frequencies, *J. Geophys. Res.*, *83*(B11), 5420–5424, doi:10.1029/JB083iB11p05420.
Aki, K. (1972), Earthquake mechanism, *Tectonophysics*, *13*, 423–446.
Aki, K., and P. G. Richards (1980), *Quantitative Seismology*, Theory and Methods, New York.
Ando, R., N. Takeda, and T. Yamashita (2012), Propagation dynamics of seismic and aseismic slip governed by fault heterogeneity and Newtonian rheology, *J. Geophys. Res.*, *117*, B11308, doi:10.1029/2012JB009532.
Armbruster, J. G., W.-Y. Kim, and A. M. Rubin (2014), Accurate tremor locations from coherent *S* and *P* waves, *J. Geophys. Res. Solid Earth*, *119*, 5000–5013, doi:10.1002/2014JB011133.
Asano, Y., K. Obara, and Y. Ito (2008), Spatiotemporal distribution of very-low frequency earthquakes in Tokachi-oki near the junction of the Kuril and Japan trenches revealed by using array signal processing, *Earth Planets Space*, *60*, 871–875.
Barbour, A. J., and D. C. Agnew (2012), Detection of seismic signals using seismometers and strain meters, *Bull. Seismol. Soc. Am.*, *102*(6), 2484–2490, doi:10.1785/0120110298.
Berger, J., P. Davis, and G. Ekström (2004), Ambient Earth noise: A survey of the Global Seismographic Network, *J. Geophys. Res.*, *109*, B11307, doi:10.1029/2004JB003408.
Bostock, M. G., A. A. Royer, E. H. Hearn, and S. M. Peacock (2012), Low frequency earthquakes below southern Vancouver Island, *Geochem. Geophys. Geosyst.*, *13*, Q11007, doi:10.1029/2012GC004391.
Bostock, M. G., A. M. Thomas, G. Savard, L. Chuang, and A. M. Rubin (2015), Magnitudes and moment-duration scaling of low-frequency earthquakes beneath southern Vancouver Island, *J. Geophys. Res. Solid Earth*, *120*, 6329–6350, doi:10.1002/2015JB012195.
Brodsky, E. E., and J. Mori (2007), Creep events slip less than ordinary earthquakes, *Geophys. Res. Lett.*, *34*, L16309, doi:10.1029/2007GL030917.
Brown, J. R., G. C. Beroza, S. Ide, K. Ohta, D. R. Shelly, S. Y. Schwartz, W. Rabbel, M. Thorwart, and H. Kao (2009), Deep low-frequency earthquakes in tremor localize to the plate interface in multiple subduction zones, *Geophys. Res. Lett.*, *36*, L19306, doi:10.1029/2009GL040027.

Brune, J. N. (1970), Tectonic stress and the spectra of seismic shear waves from earthquakes, *J. Geophys. Res.*, *75*(26), 4997–5009, doi:10.1029/JB075i026p04997.
Brune, J. N. (1971), Correction to Tectonic stress and the spectra, of seismic shear waves from earthquakes, *J. Geophys. Res.*, *76*, 5002, doi:10.1029/JB076i020p05002.
Chamberlain, C. J., D. R. Shelly, J. Townend, and T. A. Stern (2014), Low-frequency earthquakes reveal punctuated slow slip on the deep extent of the Alpine Fault, New Zealand, *Geochem. Geophys. Geosyst.*, *15*, 2984–2999, doi:10.1002/2014GC005436.
Dixon, T. H., Y. Jiang, R. Malservisi, R. McCaffrey, N. Voss, M. Protti, and V. Gonzalez (2014), Earthquake and tsunami forecasts: Relation of slow slip events to subsequent earthquake rupture, *Proc. Natl. Acad. Sci. U.S.A.*, *111*(48), 17,039–17,044, doi:10.1073/pnas.1412299111.
Fletcher, J. B., and A. McGarr (2011), Moments, magnitudes, and radiated energies of non-volcanic tremor near Cholame, CA, from ground motion spectra at UPSAR, *Geophys. Res. Lett.*, *38*, L16314, doi:10.1029/2011GL048636.
Frank, W. B., N. M. Shapiro, V. Kostoglodov, A. L. Husker, M. Campillo, J. S. Payero, and G. A. Prieto (2013), Low-frequency earthquakes in the Mexican Sweet Spot, *Geophys. Res. Lett.*, *40*, 2661–2666, doi:10.1002/grl.50561.
Frank, W. B., N. Shapiro, A. Husker, V. Kostoglodov, A. Romanenko, and M. Campillo (2014), Using systematically characterized low frequency earthquakes as a fault probe in Guerrero, Mexico, *J. Geophys. Res. Solid Earth*, *119*, 7686–7700, doi:10.1002/2014JB011457.
Frank, W. B., N. M. Shapiro, A. L. Husker, V. Kostoglodov, A. A. Gusev, and M. Campillo (2016), The evolving interaction of low-frequency earthquakes during transient slip, *Sci. Adv.*, *2*(4), e1501616, doi:10.1126/sciadv.1501616.
Frankel, A. (1995), Simulating strong motions of large earthquakes using recordings of small earthquakes: The Loma Prieta main shock as a test case, *Bull. Seismol. Soc. Am.*, *85*, 1144–1160.
Gao, H., D. A. Schmidt, and R. J. Weldon (2012), Scaling relationships of source parameters for slow slip events, *Bull. Seismol. Soc. Am.*, *102*(1), 352–360, doi:10.1785/0120110096.
Gardonio, B., D. Marsan, O. Lengliné, B. Enescu, M. Bouchon, and J.-L. Got (2015), Changes in seismicity and stress loading on subduction faults in the Kanto region, Japan, 2011–2014, *J. Geophys. Res. Solid Earth*, *120*, 2616–2626, doi:10.1002/2014JB011798.
Ghosh, A., E. Huesca-Pérez, E. E. Brodsky, and Y. Ito (2015), Very low frequency earthquakes in Cascadia migrate with tremor, *Geophys. Res. Lett.*, *42*, 3228–3232, doi:10.1002/2015GL063286.
Gomberg, J., K. Creager, J. Sweet, J. Vidale, A. Ghosh, and A. Hotovec (2012), Earthquake spectra and near-source attenuation in the Cascadia subduction zone, *J. Geophys. Res.*, *117*, B05312, doi:10.1029/2011JB009055.
Hartzell, S., S. Harmsen, A. Frankel, and S. Larsen (1999), Calculation of broadband time histories of ground motion: Comparison of methods and validation using strong-ground motion from the 1994 Northridge earthquake, *Bull. Seismol. Soc. Am.*, *89*, 1484–1504.
Hotovec, A. J., S. G. Prejean, J. E. Vidale, and J. Gomberg (2013), Strongly gliding harmonic tremor during the 2009 eruption of Redoubt volcano, *J. Volcanol. Geotherm. Res.*, *259*(C), 89–99, doi:10.1016/j.jvolgeores.2012.01.001.
Hutchison, A. A., and A. Ghosh (2016), Very low frequency earthquakes spatiotemporally asynchronous with strong tremor during the 2014 episodic tremor and slip event in Cascadia, *Geophys. Res. Lett.*, *43*, 6876–6882, doi:10.1002/2016GL069750.
Ide, S. (2008), A Brownian walk model for slow earthquakes, *Geophys. Res. Lett.*, *35*, L17301, doi:10.1029/2008GL034821.
Ide, S. (2014), Modeling fast and slow earthquakes at various scales, *Proc. Jpn. Acad. Ser. B*, *90*(8), 259–277, doi:10.2183/pjab.90.259.
Ide, S. (2016), Characteristics of slow earthquakes in the very low frequency band: Application to the Cascadia subduction zone, *J. Geophys. Res. Solid Earth*, *121*, doi:10.1002/2016JB013085.
Ide, S., and S. Yabe (2014), Universality of slow earthquakes in the very low frequency band, *Geophys. Res. Lett.*, *41*, 2786–2793, doi:10.1002/2014GL059712.
Ide, S., D. R. Shelly, and G. C. Beroza (2007a), Mechanism of deep low frequency earthquakes: Further evidence that deep non-volcanic tremor is generated by shear slip on the plate interface, *Geophys. Res. Lett.*, *34*, L03308, doi:10.1029/2006GL028890.
Ide, S., G. C. Beroza, D. R. Shelly, and T. Uchide (2007b), A scaling law for slow earthquakes, *Nature*, *447*(7140), 76–79, doi:10.1038/nature05780.
Ide, S., K. Imanishi, Y. Yoshida, G. C. Beroza, and D. R. Shelly (2008), Bridging the gap between seismically and geodetically detected slow earthquakes, *Geophys. Res. Lett.*, *35*, L10305, doi:10.1029/2008GL034014.
Ito, Y., and K. Obara (2006a), Dynamic deformation of the accretionary prism excites very low frequency earthquakes, *Geophys. Res. Lett.*, *33*, L02311, doi:10.1029/2005GL025270.
Ito, Y., and K. Obara (2006b), Very low frequency earthquakes within accretionary prisms are very low stress-drop earthquakes, *Geophys. Res. Lett.*, *33*, L09302, doi:10.1029/2006GL025883.
Ito, Y., K. Obara, K. Shiomi, S. Sekine, and H. Hirose (2007), Slow earthquakes coincident with episodic tremors and slow slip events, *Science*, *315*(5811), 503–506, doi:10.1126/science.1134454.
Ito, Y., K. Obara, T. Matsuzawa, and T. Maeda (2009), Very low frequency earthquakes related to small asperities on the plate boundary interface at the locked to aseismic transition, *J. Geophys. Res.*, *114*, B00A13, doi:10.1029/2008JB006036.
Jiang, Y., S. Wdowinski, T. H. Dixon, M. Hackl, M. Protti, and V. Gonzalez (2012), Slow slip events in Costa Rica detected by continuous GPS observations, 2002–2011, *Geochem. Geophys. Geosyst.*, *13*, Q04006, doi:10.1029/2012GC004058.
Kao, H., K. Wang, H. Dragert, J. Y. Kao, and G. Rogers (2010), Estimating seismic moment magnitude (M_w) of tremor bursts in northern Cascadia: Implications for the "seismic efficiency" of episodic tremor and slip, *Geophys. Res. Lett.*, *37*, L19306, doi:10.1029/2010GL044927.
Lengliné, O., and J.-P. Ampuero (2015), Insights on earthquake triggering processes from early aftershocks of repeating microearthquakes, *J. Geophys. Res. Solid Earth*, *120*, 6977–6992, doi:10.1002/2015JB012287.
Matsuzawa, T., K. Obara, and T. Maeda (2009), Source duration of deep very low frequency earthquakes in western Shikoku, Japan, *J. Geophys. Res.*, *114*, B00A11, doi:10.1029/2008JB006044.
McLaskey, G. C., and D. Lockner (2014), Preslip and cascade processes initiating laboratory stick slip, *J. Geophys. Res. Solid Earth*, *119*, 6323–6336, doi:10.1002/2014JB011220.
Michael, A. J. (2012), Fundamental questions of earthquake statistics, source behavior, and the estimation of earthquake probabilities from possible foreshocks, *Bull. Seismol. Soc. Am.*, *102*(6), 2547–2562, doi:10.1785/0120090184.
Nadeau, R. M., and T. V. McEvilly (1999), Fault slip rates at depth from recurrence intervals of repeating microearthquakes, *Science*, *285*, 718–721.
Ochi, T., and T. Kato (2013), Depth extent of the long-term slow slip event in the Tokai district, central Japan: A new insight, *J. Geophys. Res. Solid Earth*, *118*, 4847–4860, doi:10.1002/jgrb.50355.
Outerbridge, K. C., T. H. Dixon, S. Y. Schwartz, J. I. Walter, M. Protti, V. Gonzalez, J. Biggs, M. Thorwart, and W. Rabbel (2010), A tremor and slip event on the Cocos-Caribbean subduction zone as measured by a global positioning system (GPS) and seismic network on the Nicoya Peninsula, Costa Rica, *J. Geophys. Res.*, *115*, B10408, doi:10.1029/2009JB006845.
Peng, Z., and J. Gomberg (2010), An integrated perspective of the continuum between earthquakes and slow-slip phenomena, *Nature*, *3*(9), 599–607, doi:10.1038/ngeo940.

Protti, M. (2014), Nicoya earthquake rupture anticipated by geodetic measurement of the locked plate interface, *Nat. Geosci.*, *7*(12), 117–121, doi:10.1038/ngeo2038.

Royer, A. A., and M. G. Bostock (2014), A comparative study of low frequency earthquake templates in northern Cascadia, *Earth Planet. Sci. Lett.*, *402*(C), 247–256, doi:10.1016/j.epsl.2013.08.040.

Rubin, A. M., and J. G. Armbruster (2013), Imaging slow slip fronts in Cascadia with high precision cross-station tremor locations, *Geochem. Geophys. Geosyst.*, *14*, 5371–5392, doi:10.1002/ggge.20305.

Rubinstein, J. L., D. R. Shelly, and W. L. Ellsworth (2010), *Non-Volcanic Tremor: A Window Into the Roots of Fault Zones*, pp. 287–314, Springer, Dordrecht, Netherlands.

Savard, G., and M. G. Bostock (2015), Detection and location of low-frequency earthquakes using cross-station correlation, *Bull. Seismol. Soc. Am.*, *105*(4), 2128–2142, doi:10.1785/0120140301.

Schwartz, S. Y., and J. M. Rokosky (2007), Slow slip events and seismic tremor at circum-Pacific subduction zones, *Rev. Geophys.*, *45*, RG3004, doi:10.1029/2006RG000208.

Shelly, D. R., G. C. Beroza, S. Ide, and S. Nakamula (2006), Low-frequency earthquakes in Shikoku, Japan, and their relationship to episodic tremor and slip, *Nature*, *442*(7099), 188–191, doi:10.1038/nature04931.

Shelly, D. R., G. C. Beroza, and S. Ide (2007), Non-volcanic tremor and low-frequency earthquake swarms, *Nature*, *446*(7133), 305–307, doi:10.1038/nature05666.

Sweet, J. R., K. C. Creager, and H. Houston (2014), A family of repeating low-frequency earthquakes at the downdip edge of tremor and slip, *Geochem. Geophys. Geosyst.*, *15*, 3713–3721, doi:10.1002/2014GC005449.

Takeo, A., et al. (2010), Very broadband analysis of a swarm of very low frequency earthquakes and tremors beneath Kii Peninsula, SW Japan, *Geophys. Res. Lett.*, *37*, L06311, doi:10.1029/2010GL042586.

Thomas, A. M., G. C. Beroza, and D. R. Shelly (2016), Constraints on the source parameters of low-frequency earthquakes on the San Andreas Fault, *Geophys. Res. Lett.*, *43*, 1464–1471, doi:10.1002/2015GL067173.

Walter, J. I., S. Y. Schwartz, J. M. Protti, and V. Gonzalez (2011), Persistent tremor within the northern Costa Rica seismogenic zone, *Geophys. Res. Lett.*, *38*, L01307, doi:10.1029/2010GL045586.

Walter, J. I., S. Y. Schwartz, M. Protti, and V. Gonzalez (2013), The synchronous occurrence of shallow tremor and very low frequency earthquakes offshore of the Nicoya Peninsula, Costa Rica, *Geophys. Res. Lett.*, *40*, 1517–1522, doi:10.1002/grl.50213.

Wech, A. G., and K. C. Creager (2011), A continuum of stress, strength and slip in the Cascadia subduction zone, *Nat. Geosci.*, *4*(9), 624–628, doi:10.1038/ngeo1215.

Yamashita, Y., et al. (2015), Migrating tremor off southern Kyushu as evidence for slow slip of a shallow subduction interface, *Science*, *348*(6235), 676–679.

Zhang, J., P. Gerstoft, P. M. Shearer, H. Yao, J. E. Vidale, H. Houston, and A. Ghosh (2011), Cascadia tremor spectra: Low corner frequencies and earthquake-like high-frequency falloff, *Geochem. Geophys. Geosyst.*, *12*, Q10007, doi:10.1029/2011GC003759.